NASA TECHNICAL NOTE

NASA TN D-3157

NASA TN D-3157

TEST OF A TRUSS-CORE SANDWICH CYLINDER LOADED TO FAILURE IN BENDING

by James P. Peterson and James Kent Anderson

Langley Research Center
Langley Station, Hampton, Va.

NATIONAL AERONAUTICS AND SPACE ADMINISTRATION • WASHINGTON, D. C. • DECEMBER 1965

NASA TN D-3157

TEST OF A TRUSS-CORE SANDWICH CYLINDER LOADED TO FAILURE IN BENDING

By James P. Peterson and James Kent Anderson

Langley Research Center
Langley Station, Hampton, Va.

NATIONAL AERONAUTICS AND SPACE ADMINISTRATION

For sale by the Clearinghouse for Federal Scientific and Technical Information
Springfield, Virginia 22151 – Price $2.00

TEST OF A TRUSS-CORE SANDWICH CYLINDER LOADED TO FAILURE IN BENDING

By James P. Peterson and James Kent Anderson
Langley Research Center

SUMMARY

Results of a buckling test of a 10-foot-diameter (3-m) truss-core sandwich cylinder loaded in bending are presented. The cylinder failed as a result of the growth of wall buckles; some of the buckles existed as initial imperfections in the cylinder wall prior to testing. Failure occurred suddenly at a load corresponding to approximately 62 percent of the load computed with the use of classical small-deflection buckling theory.

INTRODUCTION

The truss-core sandwich cylinder is an attractive high-strength, low-mass structure for supporting axial loads or bending moments which induce axial compressive stresses in the wall of the cylinder. The attractiveness stems primarily from analytical studies, inasmuch as tests of sandwich structures are scarce for sandwich cylinders in general and are practically nonexistent for truss-core sandwich cylinders. Reference 1 reports the results of tests of truss-core sandwich cylinders, but the proportions of the sandwich walls of the cylinders in that investigation were derived on the basis of column theory instead of cylinder theory. As a consequence of the wall proportioning used, the elements of the walls of the cylinders buckled locally, presumably long before cylinder buckling would have occurred in the absence of elemental buckling; hence, the tests of reference 1 yielded little information on the load-carrying ability of truss-core sandwich cylinders.

The present paper reports the results of a bending test of a René 41 truss-core sandwich cylinder of all-welded construction. The cylinder was designed with the use of a contemporary cylinder analysis to be nearly optimum from a high-strength, low-mass point of view; the analysis was based on the use of classical buckling theory and a reduction factor obtained from an extrapolation of test results of conventional thin-wall cylinders. The cylinder failed as a result of wall buckling at a load of approximately 80 percent of the design load (62 percent of the classical buckling load), presumably because of imperfections in cylinder geometry which existed prior to loading.

to p. 3

SYMBOLS

The units used for the physical quantities in this paper are given both in the U.S. Customary Units and in the International System of Units (SI) (ref. 2). Appendix A presents factors relating the two systems of units used in the present investigation.

D_x, D_y	bending stiffnesses of cylinder wall in axial and circumferential directions, respectively
D_{xy}	twisting stiffness of cylinder wall
E	Young's modulus
E_x, E_y	extensional stiffnesses of cylinder wall in axial and circumferential directions, respectively
G_{xy}	shear stiffness of cylinder wall
h	depth of sandwich wall measured between centroids of two face sheets
k_x	buckling coefficient, $\frac{N_x l^2}{\pi^2 D_x}\left(1 - \mu_x \mu_y\right)$
l	length of cylinder
m	integer
M	applied moment on cylinder
M_{cr}	applied moment on cylinder at collapse
N	axial load per unit length of cylinder circumference
N_x	axial load per unit length of cylinder circumference at buckling, as given by classical theory
N_{test}	axial load per unit length of cylinder circumference at failure (buckling) of cylinder and at circumferential station of highest compressive stress ($\theta = 0$)
R	radius of cylinder
t_s	thickness of face sheet of sandwich
t_w	thickness of sheet material of core of sandwich
w	lateral deflection of cylinder wall

x,y coordinates of cylinder wall in axial and circumferential directions, respectively

Z curvature parameter, $\sqrt{\frac{E_y l^4}{R^2 D_x}(1 - \mu_x \mu_y)}$

β ratio of cylinder length to half-wavelength of buckle in circumferential direction, $\frac{l}{\lambda}$

θ angle defining distance along circumference of cylinder from generator of maximum compression stress

λ half-wavelength of buckle in circumferential direction

μ_x,μ_y Poisson's ratios of sandwich wall associated with bending of wall in axial and circumferential directions, respectively

μ_x',μ_y' Poisson's ratios of sandwich wall associated with stretching of wall in axial and circumferential directions, respectively

TEST SPECIMEN

The test specimen consisted of a René 41 all-welded truss-core sandwich cylinder approximately 10 feet (3 m) in diameter. The face sheets of the sandwich were seam welded to a corrugated core (see figs. 1 and 2) with resistance-formed spot welds spaced approximately 1/8 inch (3 mm) apart. The walls were fabricated in 18° segments which extended the entire length of the cylinder. The inside face sheet was welded to the core with the panel in a flat position and without the use of mandrels. Copper mandrels were used in welding the outside face sheet to the core; the panel was held in a contoured position during this operation. After the mandrels were removed by pulling, the panel contour deviated somewhat from the desired shape. This deviation was corrected by loading the panel with lateral loads and by peening (sandblasting) the panel with glass beads.

The panels were welded together along longitudinal joints (see fig. 1) with rodless tungsten inert gas welding; the joints had been previously machine fitted. The joints were welded from both the inside and the outside of the cylinder. The cylinder test section was terminated at each end by formed hat-section rings which were fusion spotwelded to the inside face sheet of the cylinder. The scalloped doublers at each end of the cylinder are outside the test section; they were fusion spotwelded to both the inside and outside face sheets of the cylinder to prevent local buckling and possible failure of the cylinder near the ends from stress concentrations at these locations.

The complete cylinder was heat-treated and stress-relieved after fabrication by heating in an argon-purged atmosphere at 1650° F (1172° K) for 4 hours,

air-cooling to room temperature, heating to 1400° F (1033° K) for 16 hours, and again air-cooling to room temperature.

As a result of weld shrinkage, particularly that from welding heavy adaptor rings to each end of the test cylinder, the unloaded cylinder had a slight barrel-like shape with various other imperfections superimposed upon the barrel shape. A contour map of the area of the test cylinder subsequently loaded in compression is given in figure 3. The map indicates that imperfections on the order of one-half the wall thickness are prevalent. (The average wall thickness is 0.242 in. (0.615 cm).) Figure 3 was constructed from measurements made with the use of a dial gage that was magnetically attached to a straightedge which rested against machined end fixtures at each end of the cylinder. The dial gage could be moved along the straightedge. In a reading position, the plunger of the dial gage rested against the test cylinder, and readings of the gage indicated the distance between the cylinder wall and the straightedge. Readings of the dial gage were taken at desired locations.

Another apparent effect of weld shrinkage was the troughing of the face sheets between corrugation crests in some areas of the test cylinder. There was considerable troughing near each end of the test cylinder; however, most of the troughs did not extend beyond the hat-section rings which marked the extremities of the test section. Some troughs in the face sheets near the ends of the cylinder are visible in figure 4. Longer troughs, some of which traversed the entire length of the cylinder, were visible near longitudinal weld lines joining panel segments. Such troughs probably had a detrimental effect on the circumferential wall stiffnesses and the buckling load of the cylinder. Hence, a 54° segment of the cylinder (the largest segment without the longer troughs that could be found) was chosen as the area of the test cylinder to be subjected to the highest compressive stresses.

Photomicrographs of cross sections of the cylinder wall indicate that considerable oxidation (fig. 5(a)) and intergranular corrosion (fig. 5(b)) of the René 41 wall occurred during the heat-treating process. The photomicrograph of figure 5(a) indicates that exposed surfaces of the wall material were transformed to some other material (presumably to an oxide of nickel) during heat treating. The effect of the transformation and the intergranular corrosion on the elastic properties of the wall material was not known. Hence, results of compression tests of small coupons cut from the wall of the cylinder were used to obtain elastic properties of the wall.

Typical results of compression tests of coupons cut from the wall of the cylinder are presented in figure 6; the curves are reasonably linear in the load range of interest for the test cylinder ($N < 2$ kips/in. (350 kN/m)), but they become somewhat nonlinear at higher loads. The specimens failed abruptly as a result of local buckling (crippling) at loads corresponding to the termination of the curves. Compression tests on several coupons were conducted. The mass and thickness of each coupon were obtained prior to testing, and the thicknesses of the face sheets and core of each coupon were obtained after testing. The tested coupons were cut apart to facilitate the taking of measurements. The tests and measurements indicated the following typical values of axial wall stiffness and modulus of elasticity:

$$E_x = 1050 \text{ kips/in. } (184 \text{ MN/m})$$

and

$$E = 31\,500 \text{ ksi } (217 \text{ GN/m}^2)$$

The measured values for the sandwich depth h, the face-sheet thickness t_s, and the thickness of core material t_w are given in figure 1. A value of 0.298 pound per cubic inch (8.25 Mg/m^3) (ref. 3) was used for the density of the wall material in determining cross-sectional areas from the mass measurements of the coupons; the areas thus obtained checked with areas computed by using the measured thicknesses and the known wall geometry. In addition, the value obtained for Young's modulus checked with the tabulated value for this quantity in reference 3.

TEST PROCEDURE

The test cylinder was loaded in bending with the use of a loading frame and a hydraulic testing machine. (See fig. 7.) The heavy conical sections on either end of the test cylinder were used to adapt the 10-foot-diameter (3-m) cylinder to smaller existing fixtures. The presence of stray loads during testing was minimized insofar as practicable by employing rollers between moving surfaces and by counterbalancing the fixtures near their centers of gravity. Rollers were used between the loading frame and the floor supports as well as between the loading frame and the testing machine to allow the cylinder to shorten during loading and to help restrict the loads at the roller locations to normal loads. The rollers were casehardened, as were the surfaces against which they reacted.

Resistance-type wire strain gages were mounted in a back-to-back position at various locations on the test cylinder prior to testing, and values of the strains from the gages were recorded during the test with the use of the Langley central digital data recording facility. Data from the gages were used to determine the strain distribution in the cylinder and to help detect buckling of the cylinder.

to p. 8

TEST RESULTS

The measured strain distribution in the test cylinder is compared with the calculated distribution in figure 8. The measured strain, which was obtained by averaging the values from gages located on the inside and outside surfaces of the test cylinder, is shown for three longitudinal stations on the test cylinder. The calculated strain was obtained with the use of the previously given value of the axial wall stiffness, increased by 4 percent to account for the wall material added for core splices and wall splices (see fig. 1), and with the use of the standard beam equation, in which strain is assumed linear with cylinder depth. The measured strains are generally greater than the calculated strains

in the region of highest compressive stress (region near $\theta = 0^{o}$) with the measured values scattering about the curve for calculated strain. Values of measured strain fall somewhat below the calculated curve in regions of lower compressive stress. In addition, strain measurements were taken at a few locations on the tension side of the cylinder in the area of highest tensile stress. The values of measured strain on the tension side of the cylinder (not shown in fig. 8) were of nearly the same magnitude as those of the calculated curves in figure 8, but were of opposite sign. The agreement between calculation and test shown in figure 8 indicates that the stiffness properties of the walls of the test cylinder are known with reasonable accuracy.

Selected strain-gage data from gages mounted on the inside and outside surfaces of the test cylinder in the area of high compressive stress are given in figure 9. The data indicate that the test cylinder experienced considerable wall bending during the application of the load. In some cases, wall bending started early and increased as load was increased. (Note particularly the data from the strain gages at location 9.) A correlation of the data obtained at location 9 with the contour plot of figure 3 indicates that an imperfection (buckle) which existed before the start of loading grew with the application of the load and continued to grow until cylinder failure. Just prior to failure, the buckle configuration was such that bending stresses in the wall increased at a faster rate than membrane stresses. The observed behavior suggests that the imperfection influenced the location at which buckles developed, and perhaps influenced the load level at which failure occurred. Furthermore, observed behavior indicates that well-designed truss-core sandwich cylinders should be proportioned so that the local buckling stress of the face sheets is somewhat greater than the membrane stress at which general buckling is expected; otherwise the cylinder might be expected to fail when the combination of membrane stresses and wall-bending stresses reaches the local buckling stress of the wall. Just how much greater the local buckling stress should be for maximum efficiency must be determined from experience because it presumably depends upon how well the geometry of the cylinder approximates the desired geometry.

A photograph of the cylinder after failure is given in figure 10; the area of maximum compressive stress from the bending load is near the top in the photograph. A view from inside the cylinder is shown in figure 11, again for the area of maximum compressive stress.

The test cylinder failed at an applied moment of 24 100 in-kips (2.72 Mn-N), which corresponds to a stress of about 58 ksi (400 MN/m^2). The failing load, in terms of load per unit length of circumference at the extreme compression fiber, is plotted in figure 12 for comparison with calculations of the buckling strength of the cylinder. The ordinate of figure 12 is the ratio of the test load to the calculated buckling load, where the maximum compressive load per unit length of cylinder circumference N_{test} was determined with the use of the standard beam equation; the calculated load N_x was obtained from classical small-deflection buckling theory (eq. (A4) of ref. 4) by using the value for axial wall stiffness presented previously and by assuming that the transverse shear stiffness of the core was large. The elastic constants needed for the calculation were computed with the use of the equations of reference 5. Failure occurred at 62 percent of the calculated load N_x.

The consequences of the assumption of a large transverse shear stiffness of the core were checked by making a simple but conservative calculation. In this calculation, the transverse shear stiffnesses of the core in the axial and circumferential directions were both assumed to be equal to that given in reference 6 for the circumferential or weak direction. The calculation, which was made with the use of equation (B9) of reference 4, indicated that the assumption of a large transverse shear stiffness changed the calculated buckling load by less than 1 percent.

A check calculation was also made to assess the validity of the assumption of simply supported ends, which is inherent in the calculations discussed previously for the buckling strength of the test cylinder. The calculation was made with the use of the equations for clamped cylinders presented in appendix B; a third-order determinant was used to approximate the buckling load. The buckling load computed in this manner was approximately 4 percent greater than that computed with the assumption of simple support. Because actual end conditions of the test cylinder probably lie somewhere between clamped and simply supported, calculations based on the simple-support assumption evidently entail little error.

The abscissa of figure 12 is a generalization of the radius-thickness ratio for conventional thin-wall cylinders. This ratio has been used previously in attempts to correlate experimental data on composite structures with data on conventional thin-wall cylinders. (See refs. 7 and 8.) The solid curve in figure 12 (adapted from fig. 2 of ref. 9) represents the lower bound of NASA test data on buckling of conventional thin-wall cylinders in bending; it was used in the design of the test cylinder. The dashed curve represents the lower bound of test data on buckling of conventional thin-wall cylinders from various sources; it was adapted from equation (11) of reference 10.

The circular symbol denoting the test cylinder (fig. 12) lies considerably below the curve for NASA tests and just above the curve which represents the lower limit of data from various sources. By contrast, reference 8 presents results from recent tests of honeycomb sandwich cylinders which agreed well with the curve for NASA tests on conventional cylinders. The sandwich test cylinders of reference 8 were reasonably devoid of imperfections resembling buckles; the present test cylinder was not, and the imperfections are believed to account for the comparatively low failing load of the present cylinder.

Initial imperfections in the test cylinder were evidently as damaging as those existing in the most poorly constructed of the conventional thin-wall cylinders from which the dashed curve of figure 12 was derived. The fact that imperfections in the test cylinder were readily measurable suggests that it may be possible to correlate the buckling strength of sandwich cylinders, which have considerably thicker walls than conventional thin-wall cylinders, with initial imperfections. However, such a task has proved rather formidable for thin-wall cylinders. As a result, use has been made of design procedures which account for imperfections in only a general way - for example, the two design curves of figure 12.

CONCLUDING REMARKS

The results of a buckling test of a truss-core sandwich cylinder loaded in bending are presented and discussed. The cylinder failed as a result of the growth of wall buckles, some of which existed as measurable initial imperfections before the start of loading. The cylinder failed at a load corresponding to approximately 62 percent of the load predicted on the basis of classical small-deflection buckling theory. This discrepancy between theory and test is comparable to that which would be obtained by an extrapolation of the lower limit of buckling data from various sources on conventional thin-wall cylinders.

Langley Research Center,
National Aeronautics and Space Administration,
Langley Station, Hampton, Va., August 19, 1965.

APPENDIX A

CONVERSION OF U.S. CUSTOMARY UNITS TO SI UNITS

The International System of Units (SI) was adopted by the Eleventh General Conference on Weights and Measures, Paris, October 1960, in Resolution No. 12 (ref. 2). Conversion factors for the units used herein are given in the following table:

Physical quantity	U.S. Customary Unit	Conversion factor (*)	SI unit
Density	$lbm/in.^3$	27.68×10^3	kilograms/meter^3 (kg/m^3)
Length	ft	0.3048	meters (m)
	in.	0.0254	meters (m)
Load per unit length; stiffness per unit length	kips/in.	1.751×10^5	newtons/meter (N/m)
Moment	in-kips	113.0	meter-newtons (m-N)
Stress; modulus	ksi	6.895×10^6	newtons/meter^2 (N/m^2)
Temperature	(^oF + 460)	5/9	degrees Kelvin (^oK)

*Multiply value given in U.S. Customary Unit by conversion factor to obtain equivalent value in SI unit.

Prefixes to indicate multiples of units are as follows:

Prefix	Multiple
giga (G)	10^9
mega (M)	10^6
kilo (k)	10^3
centi (c)	10^{-2}
milli (m)	10^{-3}

APPENDIX B

DERIVATION OF COMPRESSIVE BUCKLING COEFFICIENTS FOR ORTHOTROPIC CYLINDERS WITH CLAMPED ENDS

The equation of equilibrium governing the buckling of orthotropic cylinders subjected to axial compression, if deflections from transverse shear are neglected, is (see ref. 11)

$$L_D w + \frac{G_{xy}}{R^2} L_E^{-1} \frac{\partial^4 w}{\partial x^4} + N_x \frac{\partial^2 w}{\partial x^2} = 0 \tag{B1}$$

where

$$L_D = \frac{D_x}{1 - \mu_x \mu_y} \frac{\partial^4}{\partial x^4} + \left(\frac{\mu_y D_x}{1 - \mu_x \mu_y} + 2D_{xy} + \frac{\mu_x D_y}{1 - \mu_x \mu_y} \right) \frac{\partial^4}{\partial x^2 \partial y^2} + \frac{D_y}{1 - \mu_x \mu_y} \frac{\partial^4}{\partial y^4} \tag{B2}$$

$$L_E = \frac{G_{xy}}{E_y} \frac{\partial^4}{\partial x^4} + \left(1 - \mu_x' \frac{G_{xy}}{E_x} - \mu_y' \frac{G_{xy}}{E_y} \right) \frac{\partial^4}{\partial x^2 \partial y^2} + \frac{G_{xy}}{E_x} \frac{\partial^4}{\partial y^4} \tag{B3}$$

and

$$L_E^{-1} \left(L_E w \right) = w \tag{B4}$$

Equation (B1) may be solved for the buckling load by the Galerkin method. (See ref. 12.) In this method, the equilibrium equation (eq. (B1)) is represented as

$$Q(w) = 0 \tag{B5}$$

where

$$Q = L_D + \frac{G_{xy}}{R^2} L_E^{-1} \frac{\partial^4}{\partial x^4} + N_x \frac{\partial^2}{\partial x^2}$$

The deflection function is taken as

$$w = \sum_{m=1}^{\infty} a_m V_m \tag{B6}$$

where the set of functions V_m must satisfy the boundary conditions but need not satisfy the equilibrium equation. The coefficients a_m are determined from the equation

$$\int_0^{2\lambda} \int_0^{l} V_m \, Q(w) \, dx \, dy = 0 \tag{B7}$$

The following deflection function satisfies boundary conditions for clamped ends (see ref. 12):

$$w = \sin \frac{\pi y}{\lambda} \sum_{m=1}^{\infty} a_m \left[\cos \frac{(m-1)\pi x}{l} - \cos \frac{(m+1)\pi x}{l} \right] \tag{B8}$$

where V_m is seen to be

$$V_m = \sin \frac{\pi y}{\lambda} \left[\cos \frac{(m-1)\pi x}{l} - \cos \frac{(m+1)\pi x}{l} \right] \tag{B9}$$

Substituting equations (B8) and (B9) into equation (B7) and integrating over the indicated limits yields the following equations:

$$\left.\begin{aligned} a_1(2M_1 + M_3) - a_3 M_3 &= 0 \qquad (m = 1) \\ a_2(M_2 + M_4) - a_4 M_4 &= 0 \qquad (m = 2) \\ a_m(M_m + M_{m+2}) - a_{m-2} M_m - a_{m+2} M_{m+2} &= 0 \qquad (m = 3,4,5,\ldots) \end{aligned}\right\} \tag{B10}$$

where

$$M_m = (m-1)^4 + \left[2\mu_y + \frac{2(1 - \mu_x \mu_y)}{D_x} D_{xy} \right] \beta^2 (m-1)^2 + \frac{D_y}{D_x} \beta^4 + \frac{Z^2}{\pi^4} \frac{(m-1)^4}{(m-1)^4 + \left(\frac{E_y}{G_{xy}} - 2\mu_y' \right) \beta^2 (m-1)^2 + \frac{E_y}{E_x} \beta^4} - (m-1)^2 k_x \qquad (m = 1,2,3,\ldots) \tag{B11}$$

and where

$$\beta = \frac{l}{\lambda}$$

APPENDIX B

$$k_x = \frac{N_x l^2}{\pi^2 D_x}\left(1 - \mu_x\mu_y\right)$$

$$Z^2 = \frac{E_y l^4}{R^2 D_x}\left(1 - \mu_x\mu_y\right)$$

In writing equation (B11), use is made of the reciprocal relationships

$$\mu_x D_y = \mu_y D_x$$

and

$$\mu_x' E_y = \mu_y' E_x$$

The condition necessary for buckling can be represented by two subdeterminants of the coefficients of equations (B10), one for a buckle pattern symmetrical about the midpoint of the cylinder and the other for an antisymmetrical buckle pattern (ref. 13):

$$\begin{array}{l|cccccccc|}
m = 1 & 2M_1 + M_3 & -M_3 & 0 & 0 & . & . & . & \\
m = 3 & -M_3 & M_3 + M_5 & -M_5 & 0 & . & . & . & \\
m = 5 & 0 & -M_5 & M_5 + M_7 & -M_7 & . & . & . & \\
m = 7 & 0 & 0 & -M_7 & M_7 + M_9 & . & . & . & = 0 \\
. & . & . & . & . & . & . & . & \\
. & . & . & . & . & . & . & . & \\
. & . & . & . & . & . & . & . &
\end{array} \qquad (B12)$$

and

$$\begin{array}{l|cccccccc|}
m = 2 & M_2 + M_4 & -M_4 & 0 & 0 & . & . & . & \\
m = 4 & -M_4 & M_4 + M_6 & -M_6 & 0 & . & . & . & \\
m = 6 & 0 & -M_6 & M_6 + M_8 & -M_8 & . & . & . & \\
m = 8 & 0 & 0 & -M_8 & M_8 + M_{10} & . & . & . & = 0 \\
. & . & . & . & . & . & . & . & \\
. & . & . & . & . & . & . & . & \\
. & . & . & . & . & . & . & . &
\end{array} \qquad (B13)$$

APPENDIX B

Equations (B12) and (B13) can be solved for the buckling coefficient k_x by assuming values of the buckle parameter β, computing the corresponding values of k_x, and minimizing k_x with respect to β. Values of β should be restricted so that an integral number of waves occurs in the circumference of the cylinder. However, inasmuch as the number of waves is usually large, β may be treated as a continuous function. The buckling coefficient may be obtained to any desired accuracy by taking a sufficiently large number of terms in equations (B12) and (B13). In reference 13, good accuracy was obtained for conventional thin-wall cylinders with clamped ends by using only a second-order determinant.

REFERENCES

1. Younger, D. G.; and Lampert, S.: An Experimental Study on Multi-Wall Structures for Space Vehicles. WADD Tech. Rept. 60-800, U.S. Air Force, Jan. 1961.

2. Mechtly, E. A.: The International System of Units - Physical Constants and Conversion Factors. NASA SP-7012, 1964.

3. Weiss, V.; and Sessler, J. G., eds.: Aerospace Structural Metals Handbook. Volume II - Non-Ferrous Alloys. ASD-TDR-63-741, Vol. II, U.S. Air Force, Mar. 1963. (Revised Mar. 1964.)

4. Stein, Manuel; and Mayers, J.: Compressive Buckling of Simply Supported Curved Plates and Cylinders of Sandwich Construction. NACA TN 2601, 1952.

5. Libove, Charles; and Hubka, Ralph E.: Elastic Constants for Corrugated-Core Sandwich Plates. NACA TN 2289, 1951.

6. Anderson, Melvin S.: Optimum Proportions of Truss-Core and Web-Core Sandwich Plates Loaded in Compression. NASA TN D-98, 1959.

7. Peterson, James P.; and Dow, Marvin B.: Compression Tests on Circular Cylinders Stiffened Longitudinally by Closely Spaced Z-Section Stringers. NASA MEMO 2-12-59L, 1959.

8. Peterson, James P.; and Anderson, James Kent: Structural Behavior and Buckling Strength of Honeycomb Sandwich Cylinders Subjected to Bending. NASA TN D-2926, 1965.

9. Peterson, James P.: Correlation of the Buckling Strength of Pressurized Cylinders in Compression or Bending With Structural Parameters. NASA TN D-526, 1960.

10. Seide, P.; Weingarten, V. I; and Morgan, E. J.: The Development of Design Criteria for Elastic Stability of Thin Shell Structures. STL/TR-60-0000-19425(AFBMD/TR-61-7), Space Technol. Lab., Inc., Dec. 31, 1960.

11. Stein, Manuel; and Mayers, J.: A Small-Deflection Theory for Curved Sandwich Plates. NACA Rept. 1008, 1951. (Supersedes NACA TN 2017.)

12. Batdorf, S. B.: A Simplified Method of Elastic-Stability Analysis for Thin Cylindrical Shells. NACA Rept. 874, 1947. (Formerly included in NACA TN's 1341 and 1342.)

13. Batdorf, S. B.; Schildcrout, Murry; and Stein, Manuel: Critical Stress of Thin-Walled Cylinders in Axial Compression. NACA Rept. 887, 1947. (Formerly NACA TN 1343.)

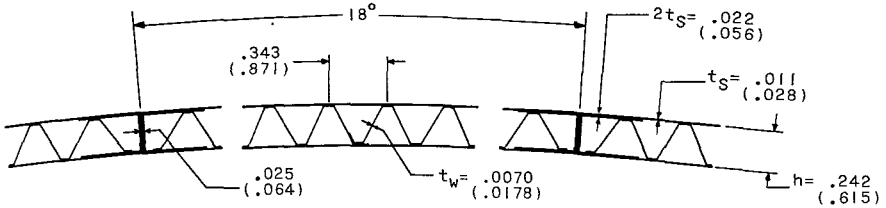

Detail A

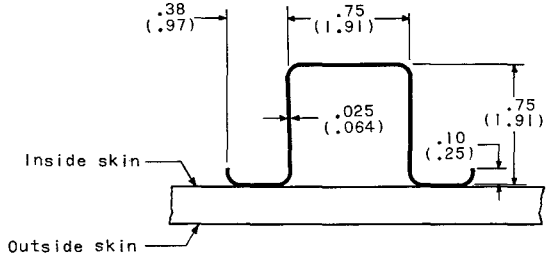

Detail B

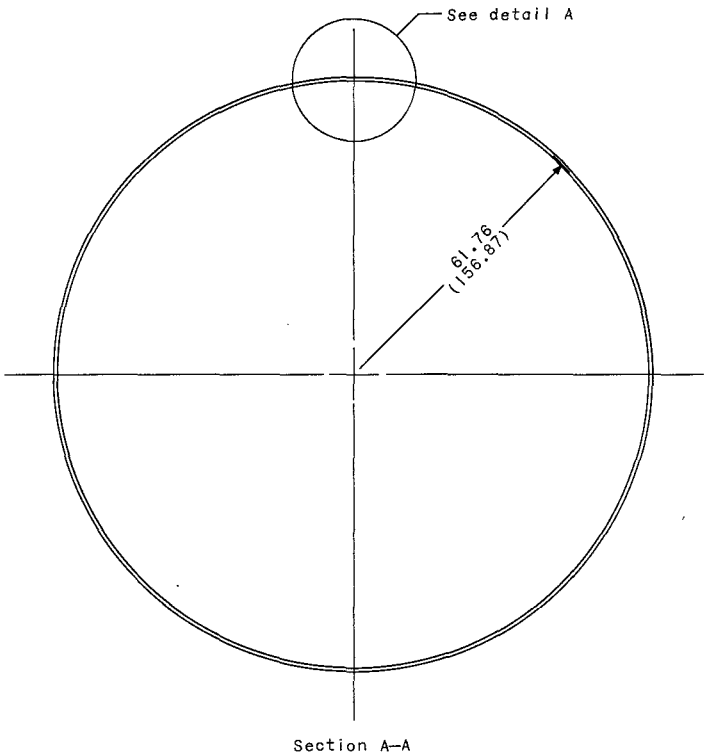

Section A–A

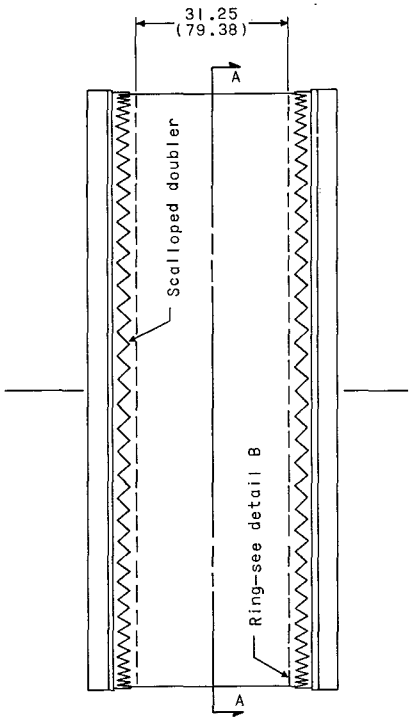

Figure 1.- Construction details of test cylinder. All dimensions are in inches. (Parenthetical dimensions are in centimeters.)

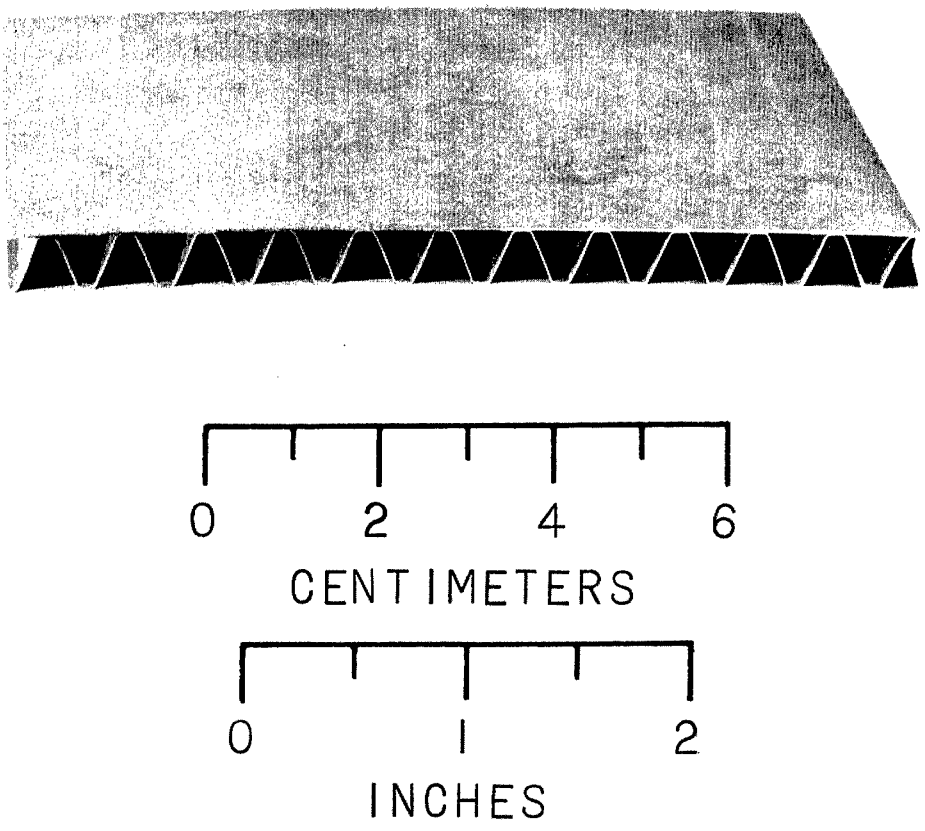

Figure 2.- Typical section from wall of test cylinder. L-65-1528

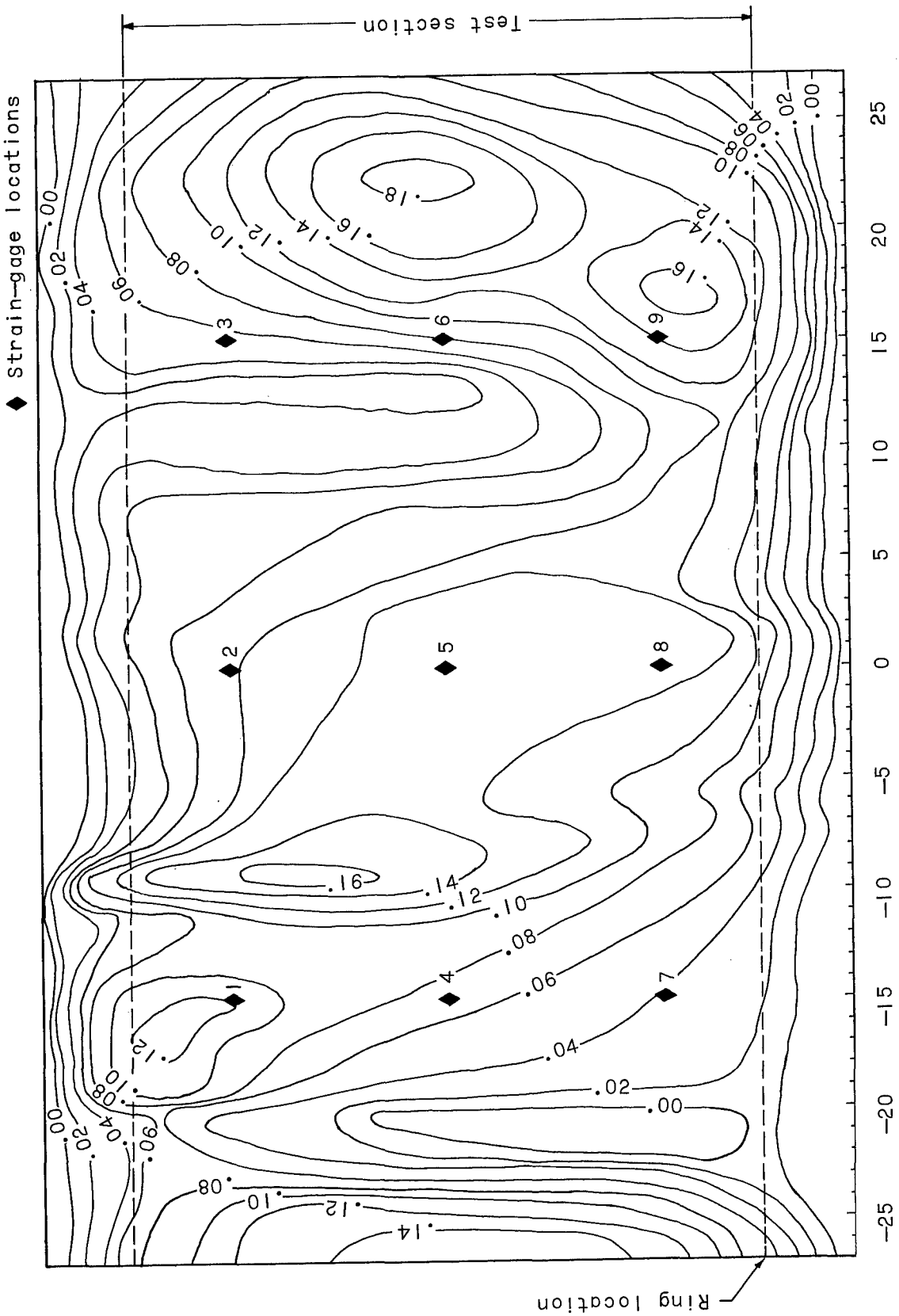

(a) Dimensions in inches.

Figure 3.- Contour map showing initial imperfections in wall of test cylinder.

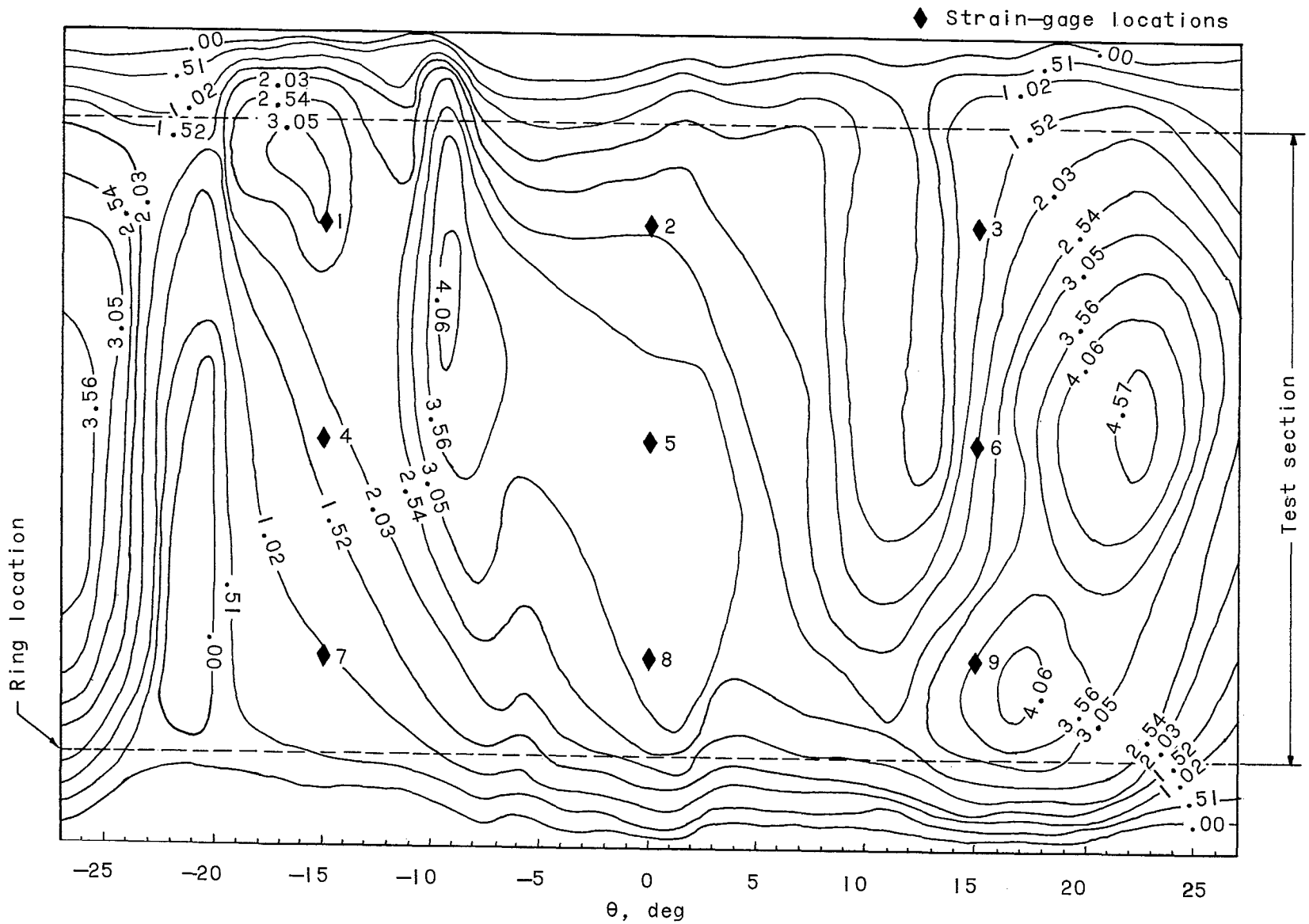

(b) Dimensions in millimeters.

Figure 3.- Concluded.

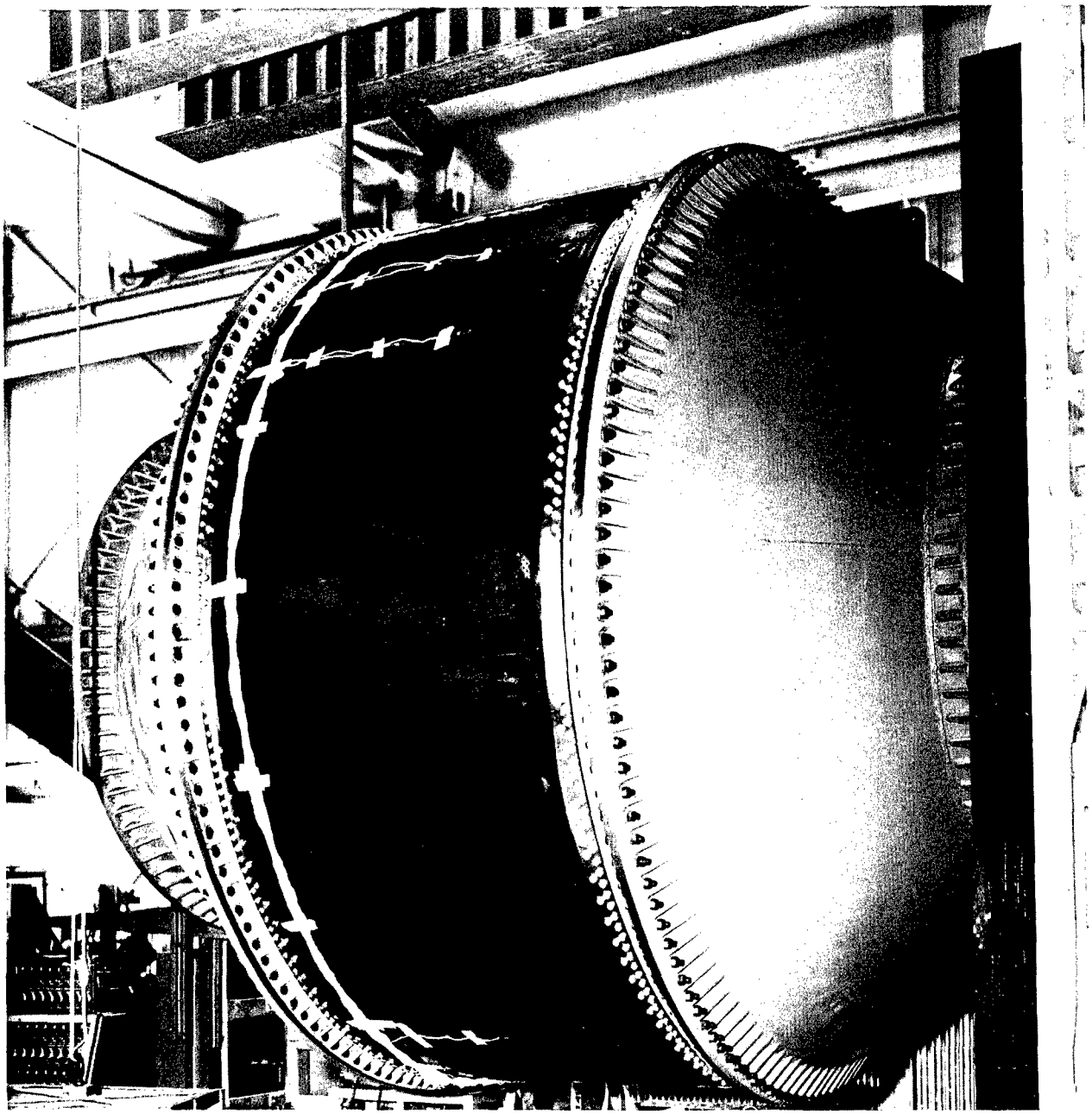

Figure 4.- Test cylinder. L-64-5778

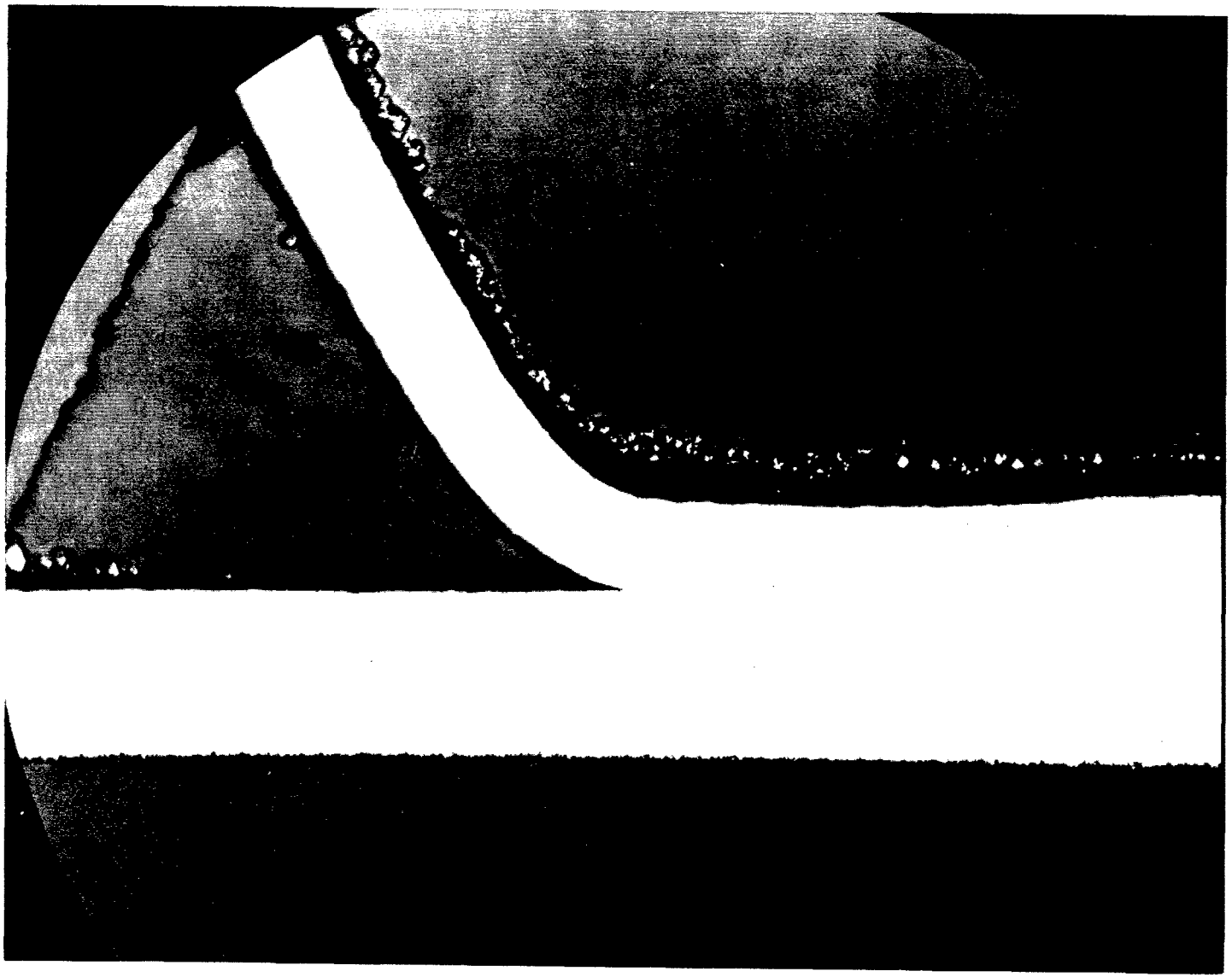

(a) Unetched.

L-65-3159

Figure 5.- Photomicrograph of section from wall of test cylinder showing oxidation and intergranular corrosion of wall. ×100.

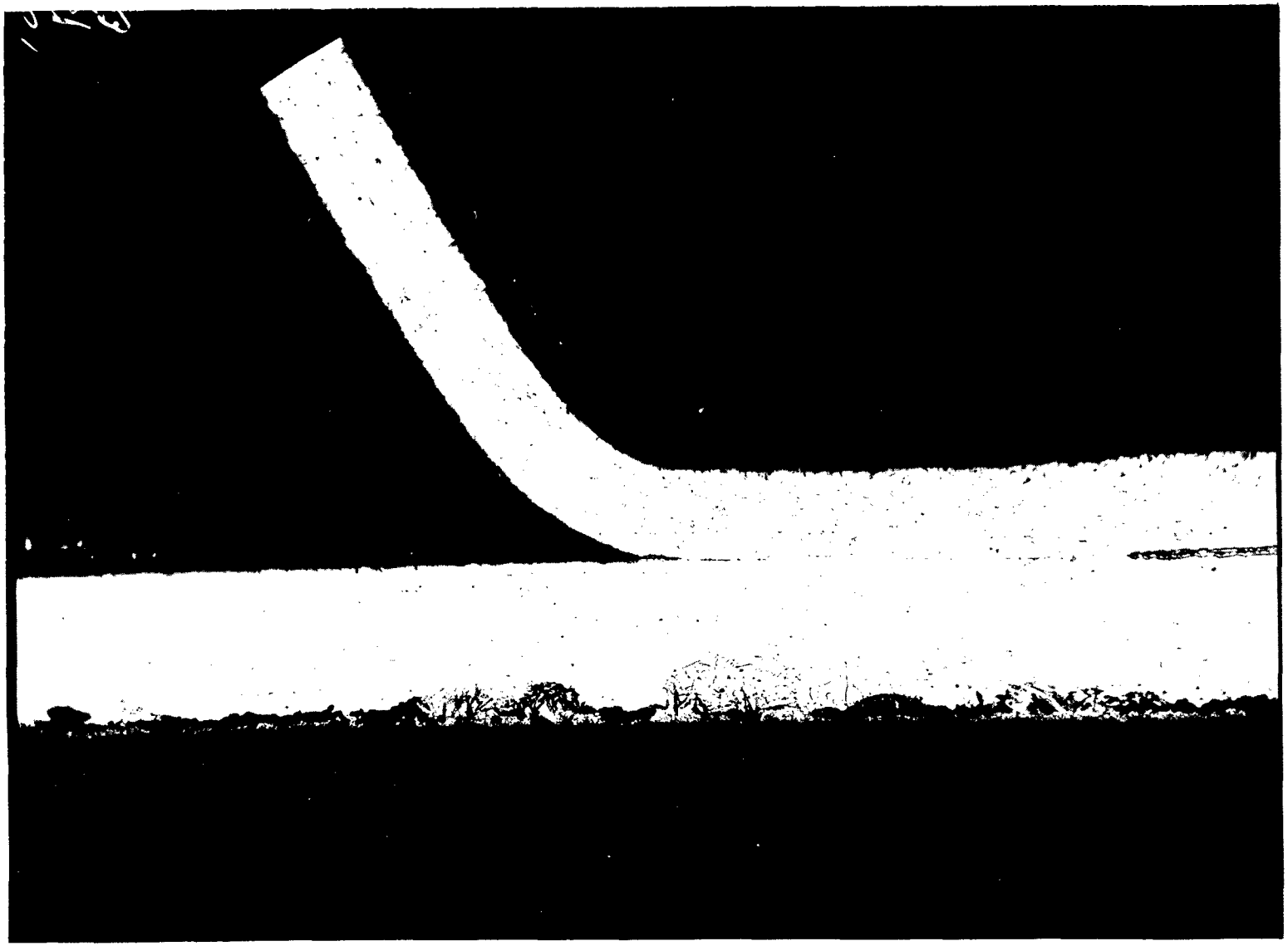

(b) Etched.

L-65-3845

Figure 5.- Concluded.

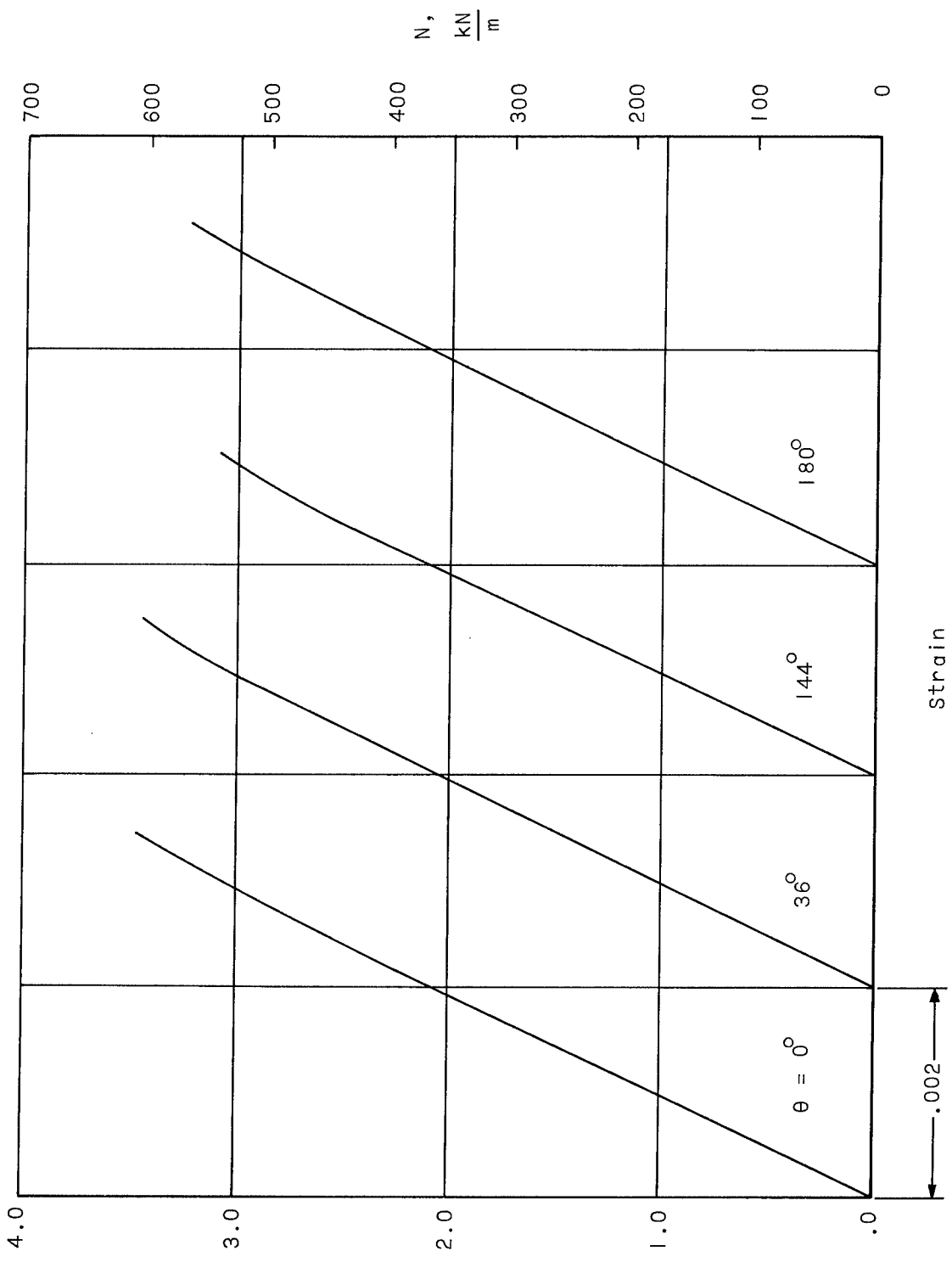

Figure 6.- Typical load-strain plots of sections from wall of test cylinder.

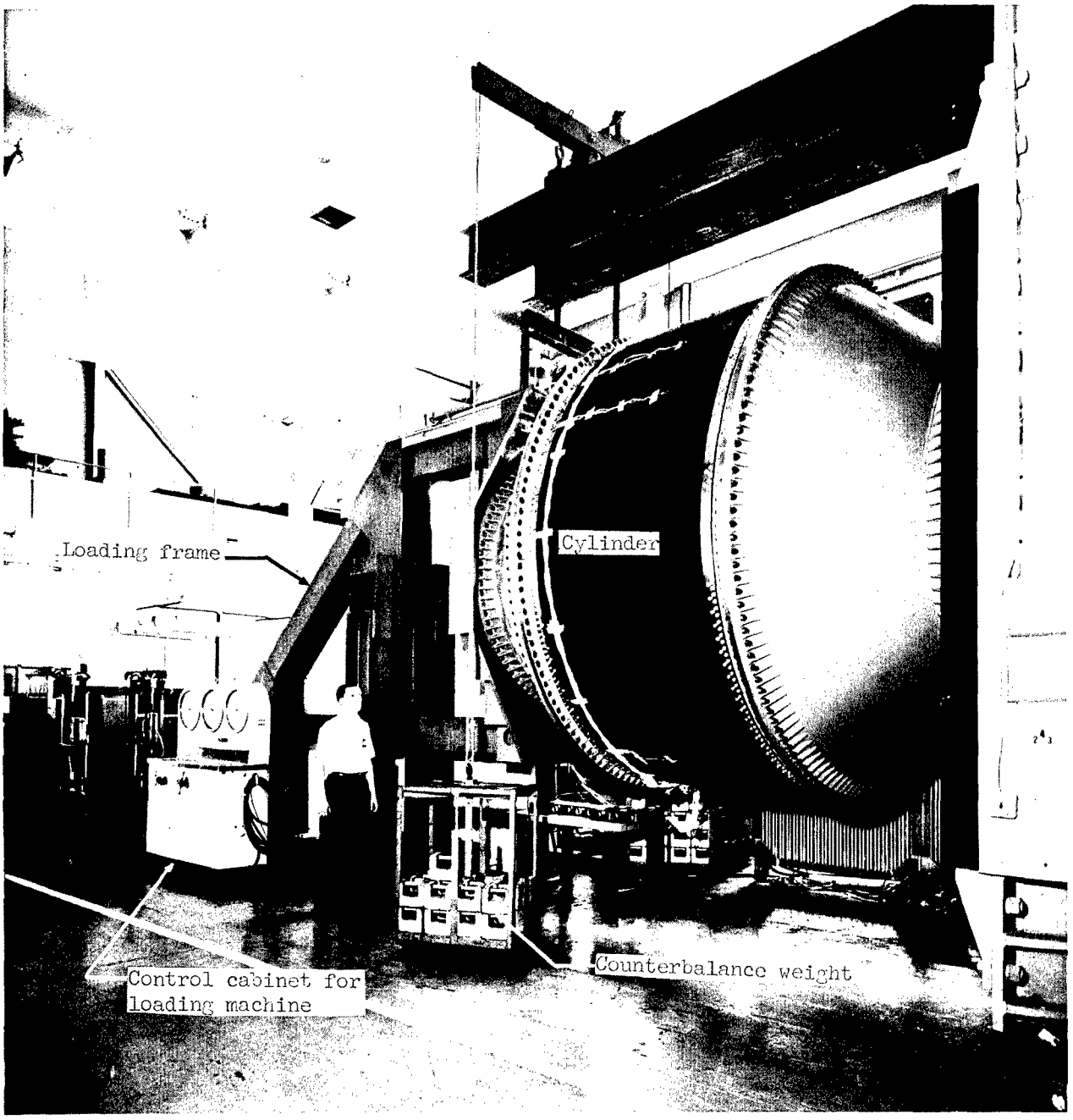

Figure 7.- Setup for bending test of sandwich cylinder. L-64-5905.1

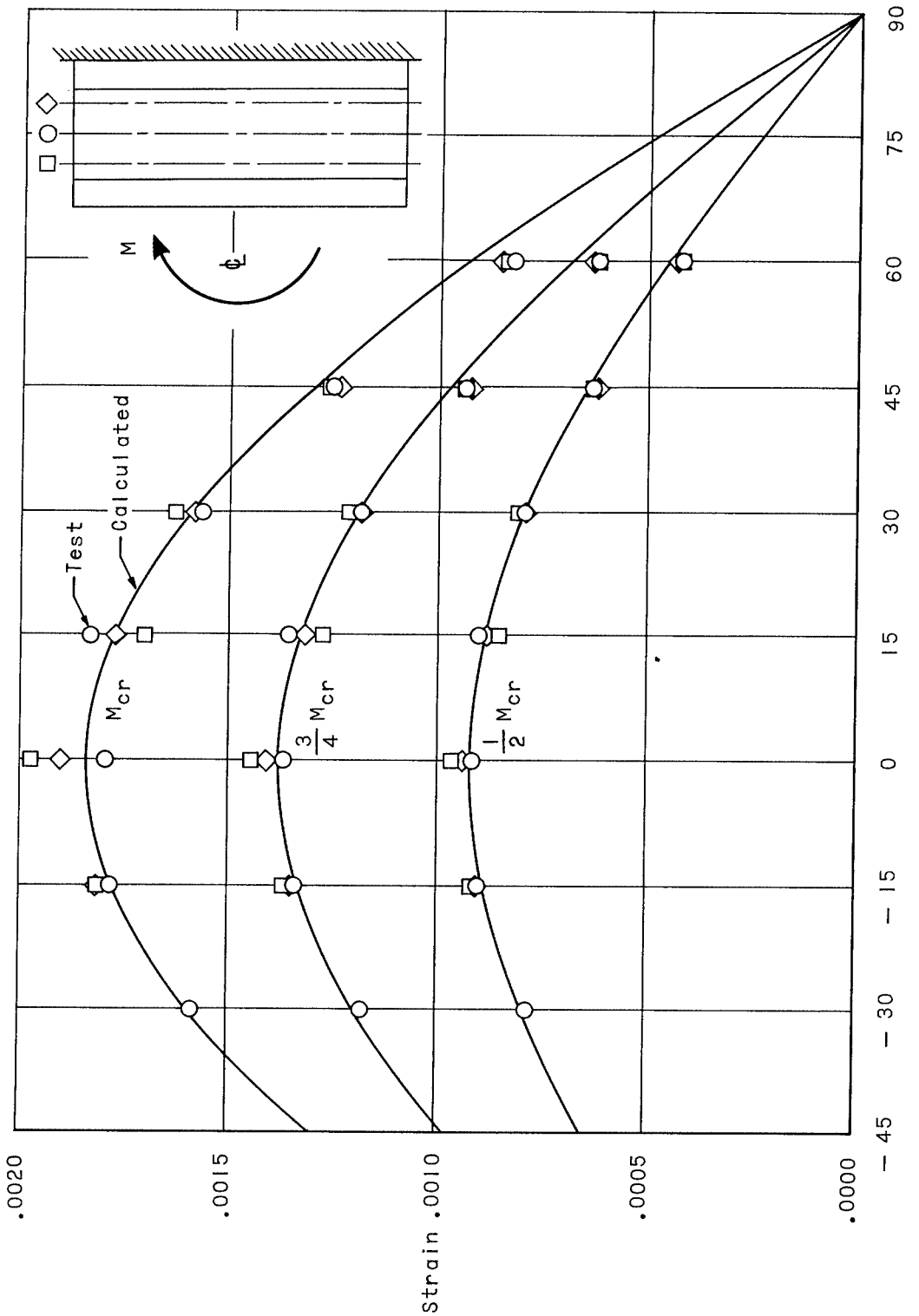

Figure 8.- Comparison between measured and calculated strain distribution in test cylinder.

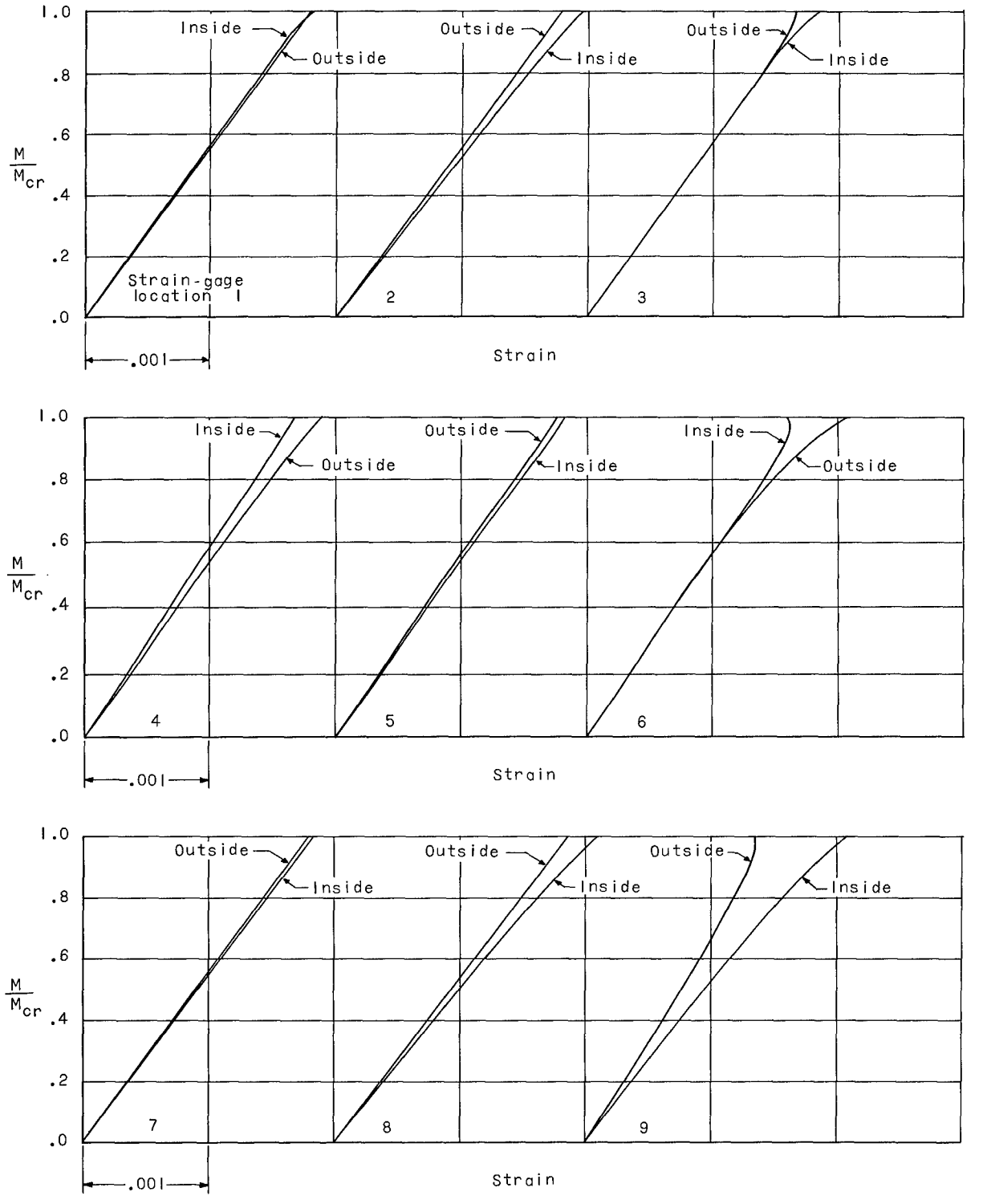

Figure 9.- Strain in test cylinder measured with strain gages mounted on inside and outside face sheets of cylinder in region of high compressive stress. See figure 3 for gage locations.

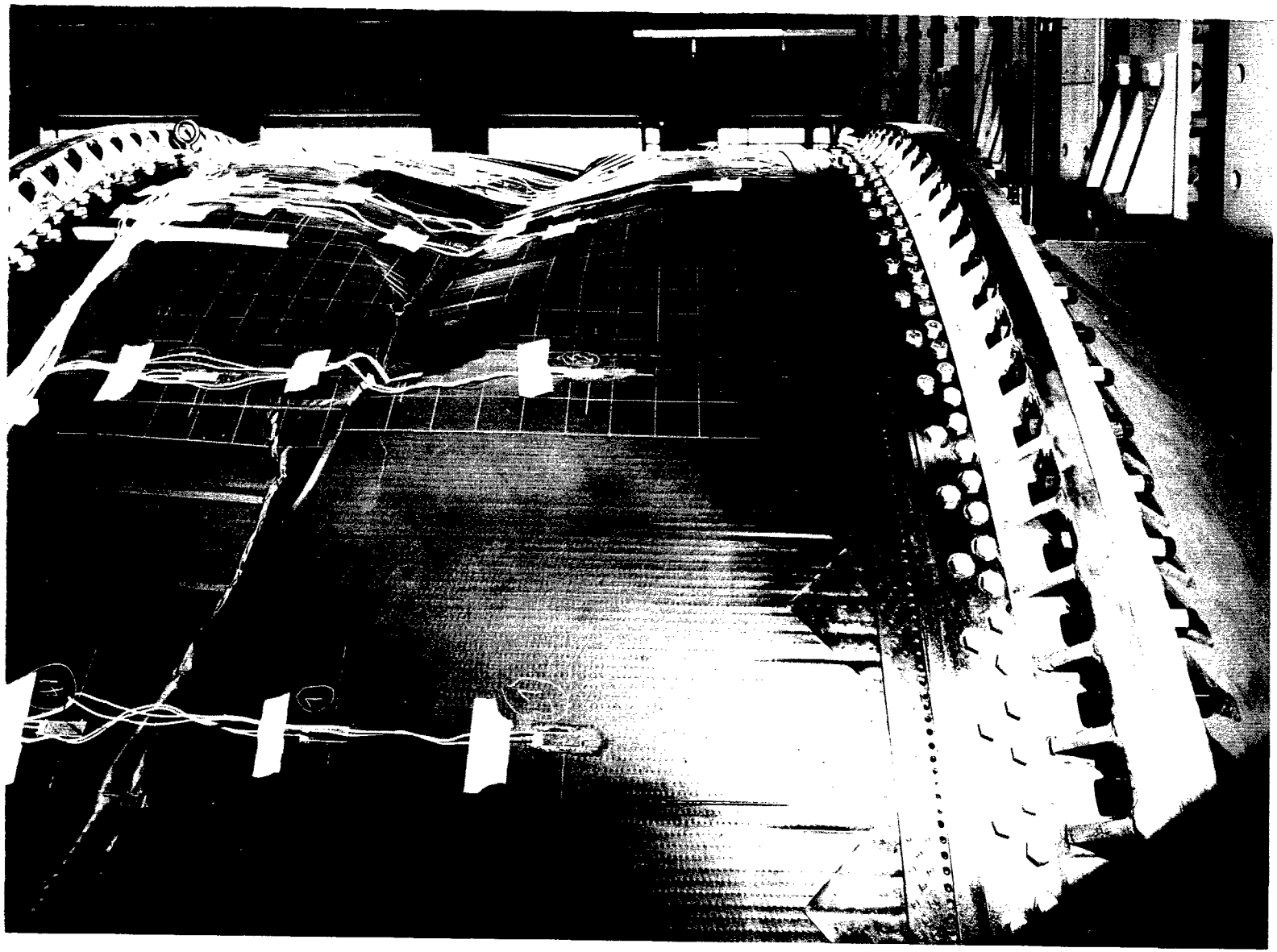

Figure 10.- Failure of test cylinder - outside view.

L-64-6181

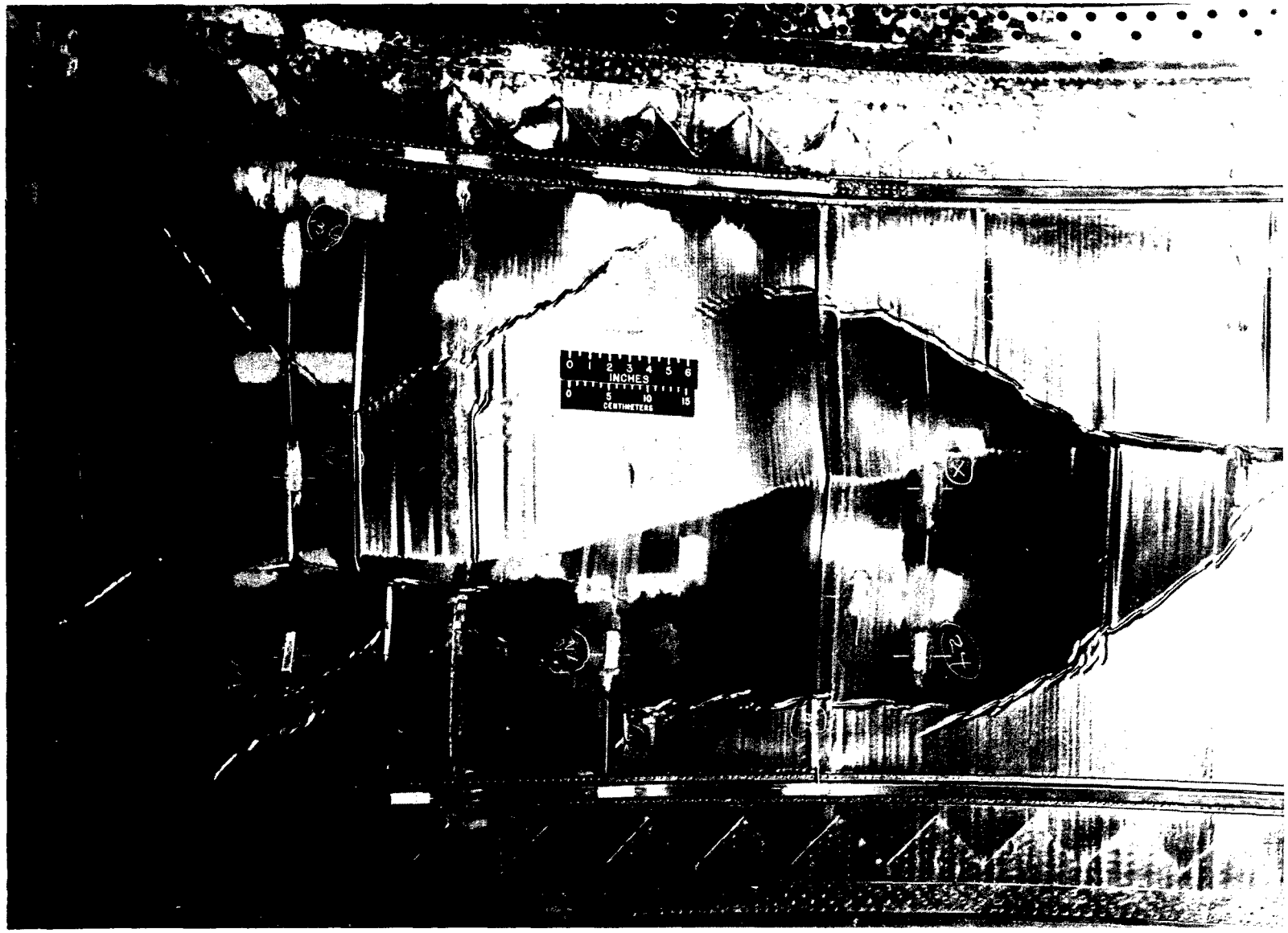

Figure 11.- Failure of test cylinder - inside view. L-64-6402

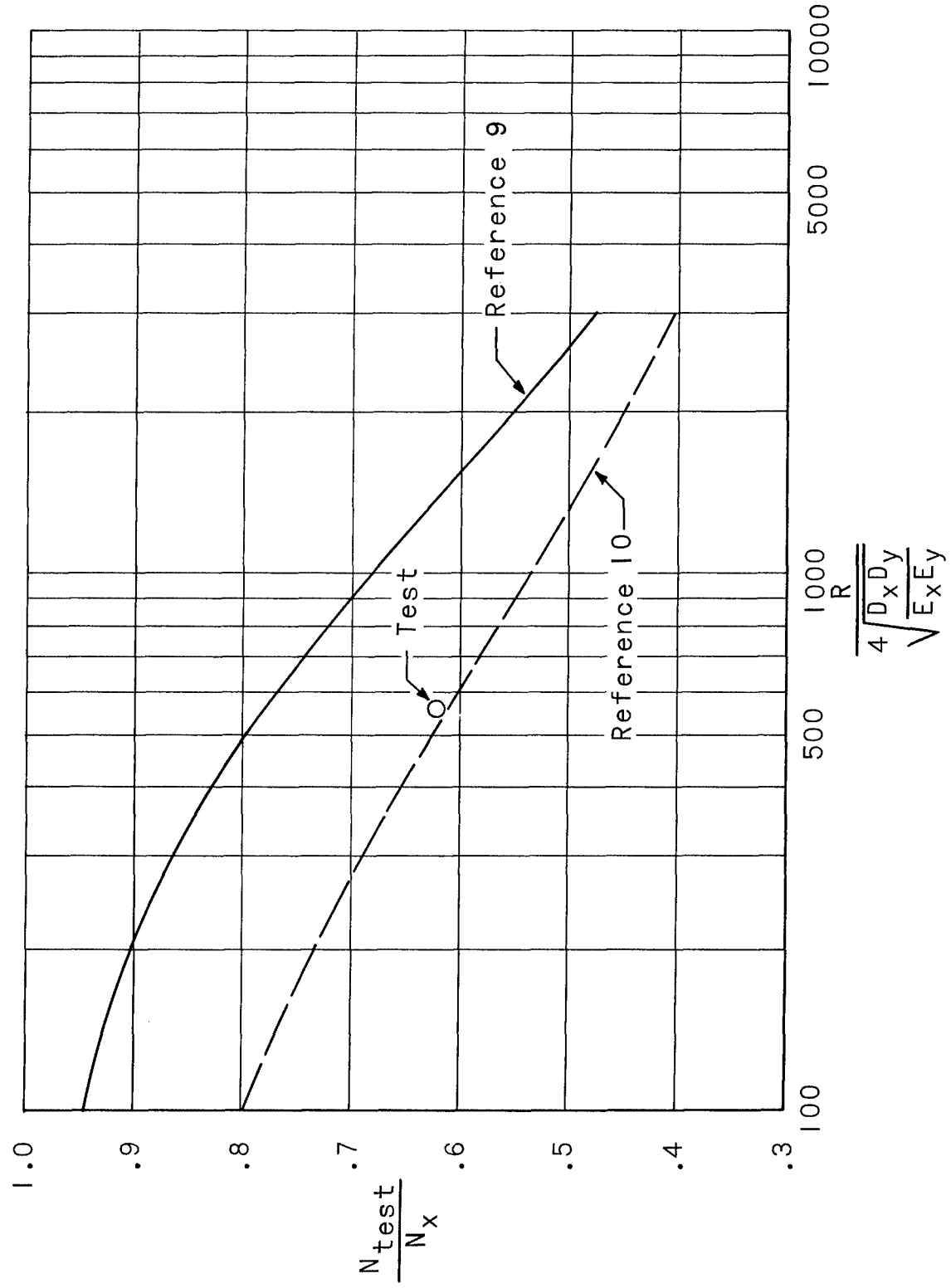

Figure 12.- Correlation of failing load of test cylinder with buckling data on conventional thin-wall cylinders.

NASA-Langley, 1965 L-4611